Iranian Journal of Science & Technology, Transaction B: Engineering, Vol. 34, No. B2, pp 117-134
Printed in The Islamic Republic of Iran, 2010

SIMULATION OF FREE SURFACE WAVE PATTERN DUE TO THE MOVING BODIES*

H. GHASSEMI[1**], M. IRANMANESH[1] AND A. ARDESHIR[2]

[1]Dept. of Marine Technology, Amirkabir University of Technology, Tehran, I. R. of Iran
[2]Dept. of Civil Engineering, Amirkabir University of Technology, Tehran, I. R. of Iran
Email: gasemi@aut.ac.ir

Abstract– Steady three-dimensional free surface waves generated by three dimensional moving bodies are presented. By applying Green's theorem and the Green function method, an integral equation for the perturbation velocity potential is obtained based on the potential flow theory. The method uses constant-strength doublet and source density distribution over the foil body surface and Neumann-type condition. On the undisturbed free surface source density is applied to satisfy the free surface condition that is defined by the first and second order solutions. After solving the doublet on the body and source on the free surface, the computational results of pressure, lift, wave drag, wave pattern and wave elevation can be calculated at various Froude numbers. The results for the surface piercing (such as strut and Wigley hull) and submerged moving hydrofoils have been presented. The validity of the numerical results is examined by comparing it with the experimental results.

Keywords– Free surface, pressure distribution, lift and drag, wave pattern, Wigley hull

1. INTRODUCTION

When a body moves near the free surface of water, a pattern of trailing gravity waves is generated. Numerical modeling of this problem is a subject of high interest for ship design and marine engineering. An illumination of such detailed mechanisms is always desirable for research in hydrodynamics. A flow characteristic may be described by two major independent parameters: the Reynolds number and the Froude number. The free surface and wave resistance can be computed with a potential theory, whereas the viscous effect can be considered by using the RANS equation.

According to linear wave flow theory, a disturbance advancing at steady speed on or below the free surface creates a so-called Kelvin wave pattern. A surface wave created by a disturbance moving at high-speed is significantly different from this theory due to nonlinearity. In such cases, it is necessary to attempt the problem by using a numerical model with nonlinear free surface conditions.

In the past, theoretical free surface and wave resistance was reviewed by Wehausen [1], Newman [2] and numerically presented by many researchers [3-8]. Very important progress has been achieved in the calculation of two-dimensional free surface waves. Forbes [6] presented a numerical algorithm for the solution of 3-D problems involving a fluid with a free surface. Recently generalizations for two submerged disturbances were also presented by Parau et al. [7]. Nakos & Sclavounos [9] pointed out such a steady flow not only yields wave resistance but also sinkage and trim, which are two significant parameters for determining ship hull power requirements and operating condition. Wave pattern and wave resistance of surface piercing bodies by a boundary element method were predicted by many researchers,

*Received by the editors March 9, 2009; Accepted October 12, 2009.
**Corresponding author

namely Bal [10], Uslu & Bal [11], Xie & Vassalos [12] and Kara et al 13], all of whom considered linearized free surface boundary condition. Recently, Ghassemi et al. [14-16] presented nonlinear free surface flow and higher order boundary element method on the various submerged (hydrofoil, strut) and surface bodies (Wigley hull). Numerical comparison of the planing mono-hull and catamaran at high Froude numbers were predicted by Seif and Amini [17].

This paper concentrates on the computation of the free surface for a body in steady motion, by means of a potential model for the fluid and a second-order nonlinearized free surface boundary condition. The governing equations are the Laplace equation with slip boundary conditions on the domain. The free surface boundary condition amounts to a Neumann boundary condition with a source term proportional to the streamlined second derivative of the potential. The method is applied to various three dimensional bodies. Some numerical results of pressure, lift, wave-making resistance and wave surface elevations are calculated at Froude number.

2. MATHEMATICAL FORMULATIONS

We consider three dimensional moving bodies at a constant velocity $\vec{U}$ at the surface of a fluid of infinite depth. The sketch of the body and free surface are depicted in Fig. 1. The fluid is assumed to be inviscid and incompressible and the flow to be irrotational. We choose a Cartesian frame of reference moving bodies and assume that the flow is steady. The Cartesian coordinates (x, y, z) are chosen with the z-axis directed vertically upwards and the x-axis in the opposite direction of the velocity $\vec{U}$. The equation of the free surface is denoted by $z = \zeta(x, y)$. The total potential function is introduced by $\Phi(x, y, z)$ so its velocity is given by Φ_x and Φ_y in the x and y direction, respectively. In the flow field, the total potential function $\Phi(x, y, z)$ satisfies Laplace's equation.

$$\nabla^2 \Phi = 0, \qquad x, y \in R \qquad\qquad z < \zeta(x, y) \tag{1}$$

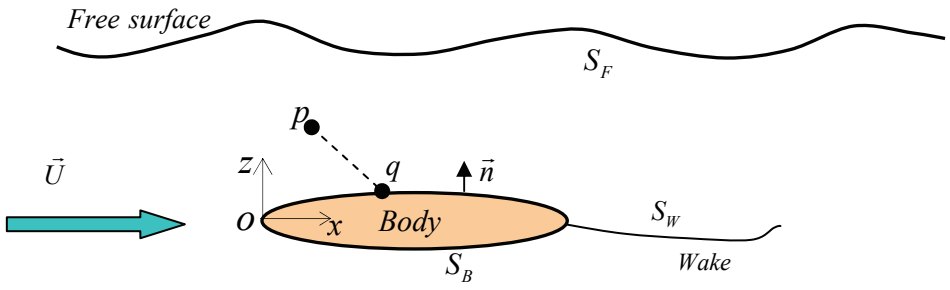

Fig. 1. Application of Green's theorem for the general body

The total velocity potential, Φ, consists of the perturbation potential, ϕ, and free stream velocity potential, ϕ_{in},:

$$\begin{cases} \Phi = \phi + \phi_{in} \\ \phi_{in} = -\vec{U} \cdot \vec{X}(p) \end{cases} \tag{2}$$

Four boundary conditions on the body and free surfaces are given as follows:

i. Kinematic boundary conditions:

$$\Phi_x \zeta_x + \Phi_y \zeta_y = \Phi_z \qquad\qquad z = \zeta(x, y) \tag{3}$$

ii. Dynamic boundary condition:

$$\frac{1}{2}\left(\Phi_x^2+\Phi_y^2+\Phi_z^2\right)+g\zeta=\frac{U^2}{2} \qquad z=\zeta(x,y) \tag{4}$$

Here, g is the acceleration of gravity and ρ is the fluid density. Combining Eqs. (3) and (4) we obtain

$$\nabla\Phi.\nabla\left[\frac{1}{2}\left(\nabla\Phi\cdot\nabla\Phi\right)\right]-g\Phi_z=0 \qquad z=\zeta(x,y) \tag{5}$$

The free-surface boundary condition (5) is nonlinear and should be satisfied on the true surface, which is unknown and can be obtained using the perturbation method. Substituting Eq. (2) in Eq. (5) and expanding the potential ϕ in a Taylor series about the mean free surface $z=0$, the first and second order free-surface boundary conditions can be obtained as follows (Tarafder & Suzuki, [18])

$$\begin{aligned} &1^{st}-order:\ \phi_{1xx}-K_0\phi_{1z}=0 \\ &2^{nd}-order:\phi_{2xx}-K_0\phi_{2z}=R_2 \end{aligned} \qquad at\quad z=0 \tag{6}$$

where $K_0=g/U^2$ is the wave number and

$$R_2=-\frac{1}{\vec{U}}\frac{\partial}{\partial x}\left(\phi_{1x}^2+\phi_{1y}^2+\phi_{1z}^2\right)-\zeta_1\frac{\partial}{\partial z}\left(\phi_{1xx}-K_0\phi_{1z}\right) \tag{7}$$

iii. Radiation condition:

The upstream radiation condition gives

$$no\ \ wave\ \ as \quad x\to+\infty \tag{8}$$

iv. Kutta condition:

An additional and very important Kutta condition for lifting bodies (hydrofoil and rudder) is required at the trailing edge to uniquely specify the circulation. It numerically states that the pressure of the back side (BS) and face side (FS) body at the trailing edge (TE) should equal, i.e.

$$\Delta P_{TE}=0\Rightarrow P_{TE}^{BS}-P_{TE}^{FS}=0 \tag{9}$$

Applying the integral representation for the perturbation potential function $\phi(p)$, Green's second identity can be written as

$$e\phi(p)=\int_{S(S_B+S_F+S_W)}\left[\phi\frac{\partial G}{\partial n}-G\frac{\partial\phi}{\partial n}\right]dS \tag{10}$$

e is the solid angle, the value of which depends on the position of the field point p in the fluid domain. If point p is placed on the boundary (body surface), then the coefficient e is replaced by 0.5. If point p is placed inside and outside of the body then the value of e is one and zero, respectively. The surfaces include body surface, S_B, free surface, S_F, and trailing vortex wake surface, S_W. Trailing vortex wake surface is considered for lifting body, which is important for satisfying the Kutta condition. Green's function for a free surface is given by

$$G=\frac{1}{4\pi}\left(\frac{1}{\vec{r}}+\frac{1}{\vec{r}'}\right) \tag{11}$$

where

$$\vec{r} = |q - p| \quad \text{and} \quad \vec{r}' = |q' - p| \tag{12}$$

$\vec{r}$ and $\vec{r}'$ are the distance between the singular point $p(x,y,z)$ and the point $q(u,v,w)$ or its image point $q'(u,v,w)$ that is integrated;

Therefore, Eq. (10) can be expressed as

$$\begin{aligned} 4\pi e\phi(p) = & \int_{S_B} \phi(q) \frac{\partial}{\partial n_q}\left(\frac{1}{r} + \frac{1}{r'}\right) dS - \int_{S_B} \frac{\partial \phi(q)}{\partial n_q}\left(\frac{1}{r} + \frac{1}{r'}\right) dS \\ & + \int_{S_W} \Delta\phi(q) \frac{\partial}{\partial n_q}\left(\frac{1}{r} + \frac{1}{r'}\right) dS - \int_{S_F} \frac{\partial \phi(q)}{\partial n_q}\left(\frac{1}{r} + \frac{1}{r'}\right) dS \end{aligned} \tag{13}$$

The right hand of the Eq. (13) has four terms. The two first terms are doublet and source on the body, the third term is the doublet on the trailing vortex wake surface (defined only for lifting bodies) and the last term is the effect of the free surface source distribution on the body.

3. THE NUMERICAL SCHEME

a) Arrangement of the matrix form

The whole surfaces (wetted body surface, free surface and trailing vortex surface) are discretized into the quadrilateral elements. The general discretized form of integral Eq. (13) for the wetted surface of the body can be expressed as

$$\begin{aligned} \phi(p_i) = & \sum_{\substack{j=1 \\ (i \neq j)}}^{N_B} \phi(q_j)\left[DB_{ij}\right] - \sum_{j=1}^{N_B}\left(\frac{\partial \phi(q)}{\partial n}\right)_j \left[SB_{ij}\right] \\ & + \sum_{j=1}^{M}\sum_{l=1}^{N_W} \Delta\phi(q_j)\left[DW_{ijl}\right] - \sum_{j=1}^{N_F}\left(\frac{\partial \phi(q)}{\partial n}\right)_j \left[SF_{ij}\right], \quad \mathrm{p}_i \in S_B) \end{aligned} \tag{14}$$

where

$$\begin{aligned} DB_{ij} &= \frac{1}{4\pi e}\int_{S_B} \frac{\partial}{\partial n}\left(\frac{1}{r_{ij}} + \frac{1}{r'_{ij}}\right) dS_j, \qquad SB_{ij} = \frac{1}{4\pi e}\int_{S_B}\left(\frac{1}{r_{ij}} + \frac{1}{r'_{ij}}\right) dS_j \\ DW_{ijl} &= \frac{1}{4\pi e}\int_{S_W} \frac{\partial}{\partial n}\left(\frac{1}{r_{ijl}} + \frac{1}{r'_{ijl}}\right) dS_l, \qquad SF_{ij} = \frac{1}{4\pi e}\int_{S_F}\left(\frac{1}{r_{ij}}\right) dS_j \end{aligned} \tag{15}$$

and N_B and N_F are the number of elements on the wetted hull and free surfaces, respectively. N_W and M are also the number of elements on the trailing vortex wake surface and spanwise of the hydrofoil or strut, respectively. The velocity component $(\partial\phi/\partial n)$ is known on the body surface from the kinematic boundary condition, while it is unknown on the free surface. This boundary condition is expressed as

$$\begin{cases} \begin{cases} 1st - order : \dfrac{\partial \phi_1}{\partial n} = \vec{U}.\vec{n} \\ 2nd - order : \dfrac{\partial \phi_2}{\partial n} = 0 \end{cases} & known \quad on \quad S_B \\ \dfrac{\partial \phi}{\partial n} = \sigma & unknown \quad on \quad S_F \end{cases} \tag{16}$$

Here, the Eqs. (14) and (6) constitute the matrix form to solve the potential and source unknowns. When the field element (p_i) is located on the free surface, means $\phi(p_i \in S_F)$, $e = 1$, substituting the Eq. (14) into Eq. (6), we have

$$\begin{aligned} 1st-Order &: \sum_{j=1}^{N_B}\phi_{1j}\frac{\partial^2[DB_{ij}]}{\partial x^2} - \sum_{j=1}^{N_B}(\vec{U}.\vec{n})_j\frac{\partial^2[SB_{ij}]}{\partial x^2} + \sum_{j=1}^{M}\sum_{j=1}^{N_W}\Delta\phi_{1j}\frac{\partial^2[DW_{ijl}]}{\partial x^2} - \sum_{j=1}^{N_F}\sigma_{1j}\left(\frac{\partial^2[SF_{ij}]}{\partial x^2} - K_0\delta_{ij}\right) = 0 \\ 2nd-order &: \sum_{j=1}^{N_B}\phi_{2j}\frac{\partial^2[DB_{ij}]}{\partial x^2} + \sum_{j=1}^{M}\sum_{j=1}^{N_W}\Delta\phi_{2j}\frac{\partial^2[DW_{ijl}]}{\partial x^2} - \sum_{j=1}^{N_F}\sigma_{2j}\left(\frac{\partial^2[SF_{ij}]}{\partial x^2} - K_0\delta_{ij}\right) + \sum_{j=1}^{N_F}R_{2j} = 0 \qquad i = 1,2,..,N_F \end{aligned} \tag{17}$$

When the field element (p_i) is located on the body surface, means $\phi(p_i \in S_B)$, $e = 0.5$, Eq. (14) is expressed as

$$\begin{aligned} 1st-order &: \sum_{j=1}^{N_B}\phi_{1j}[\delta_{ij} - DB_{ij}] - \sum_{j=1}^{N_B}(\vec{U}.\vec{n})_j[SB_{ij}] + \sum_{j=1}^{M}\sum_{j=1}^{N_W}\Delta\phi_{1j}[DW_{ijl}] - \sum_{j=1}^{N_F}\sigma_{1j}[SF_{ij}] = 0 \\ 2nd-order &: \sum_{j=1}^{N_B}\phi_{2j}[\delta_{ij} - DB_{ij}] - \sum_{j=1}^{M}\sum_{j=1}^{N_W}\Delta\phi_{2j}[DW_{ijl}] - \sum_{j=1}^{N_F}\sigma_{2j}[SF_{ij}] - \sum_{j=1}^{N_F}R_{2j} = 0 \qquad i = 1,2,..,N_B \end{aligned} \tag{18}$$

where δ_{ij} is Kronecker delta function. The total numbers of unknowns are N_B+N_F *(= N_T)*. *NB* is the number of potential (ϕ) on the wetted body surface and N_F is the number of velocity components (σ) on the free surface. The second derivative of the influence coefficients $(DB_{xx}, SB_{xx}, SF_{xx})$ are computed by four-point finite difference operator, and four-point upstream operator is also introduced to satisfy the condition of no waves propagating upstream. The matrix form of combined Eqs. (17) and (18) are expressed as

For the first-order:

$$\begin{bmatrix} [\delta - DB]_{N_B\times N_B} & [SF]_{N_B\times N_F} \\ [DB_{xx}]_{N_F\times N_B} & [-K_0\delta + SF_{xx}]_{N_F\times N_F} \end{bmatrix} \begin{Bmatrix} \{\phi_1\}_{N_B\times 1} \\ \{\sigma_1\}_{N_F\times 1} \end{Bmatrix} = \begin{bmatrix} [DW]_{N_B\times N_B} \\ [DW_{xx}]_{N_F\times N_B} \end{bmatrix} \begin{Bmatrix} \{\Delta\phi_1\}_{N_B\times 1} \\ \{0\}_{N_F\times 1} \end{Bmatrix} + \begin{bmatrix} [SB]_{N_B\times N_B} \\ [SB_{xx}]_{N_F\times N_B} \end{bmatrix} \begin{Bmatrix} \{\vec{U}.\vec{n}\}_{N_B\times 1} \\ \{0\}_{N_F\times 1} \end{Bmatrix} \tag{19}$$

For the second-order:

$$\begin{bmatrix} [\delta - DB]_{N_B\times N_B} & [SF]_{N_B\times N_F} \\ [DB_{xx}]_{N_F\times N_B} & [-K_0\delta + SF_{xx}]_{N_F\times N_F} \end{bmatrix} \begin{Bmatrix} \{\phi_2\}_{N_B\times 1} \\ \{\sigma_2\}_{N_F\times 1} \end{Bmatrix} = \begin{bmatrix} [DW]_{N_B\times N_B} \\ [DW_{xx}]_{N_F\times N_B} \end{bmatrix} \begin{Bmatrix} \{\Delta\phi_2\}_{N_B\times 1} \\ \{0\}_{N_F\times 1} \end{Bmatrix} + \begin{Bmatrix} 0 \\ \{R_2\}_{N_F\times 1} \end{Bmatrix} \tag{20}$$

Another matrix form of Eq. (19) or (20) is

$$[A]_{N_T\times N_T}\{x\}_{N_T\times 1} = \{b\}_{N_T\times 1} \tag{21}$$

For this type of problem, a formal solution may be given by the direct solution methods of *LU* decomposition or Gaussian elimination. However, the solution vector may have extensively large components whose algebraic elimination, when multiplied by the matrix ***A***, may give a poor approximation for the right-hand vector ***b***. This affects the errors in the solution of the matrix Eq. (21). In the present study, a SVD technique has been adopted to solve matrix Eq. (21).

Indexes of 1 and 2 for ϕ_1, σ_1, ϕ_2 and σ_2 represent the first and second order of ϕ and σ. The integrals over the element are calculated by numerical method [19]. The circulation $\Delta\phi$ is unknown and will be determined by satisfying the pressure Kutta condition. After getting the first-order solution, the derivatives of the velocity potentials with respect to x and y (such as ϕ_{1x}, ϕ_{1y}) of R_2 are evaluated by differentiation of potential ($\nabla\phi_1$). The derivatives of velocity potential with respect to *z* (such as ϕ_{1z}) of R_2 are obtained after calculating the velocity potentials at three consecutive points along the *z*-direction.

b) Wave profile, lift and drag

The wave profiles can be obtained by the first and second order of Taylor's series expansion as follows

$$\zeta_1 = -\frac{U}{g}\phi_{1x}$$
$$\zeta_2 = -\frac{U}{g}\phi_{2x} - \frac{U}{g}\zeta_1\phi_{1xz} - \frac{1}{2g}(\phi_{1x}^2 + \phi_{1y}^2 + \phi_{1z}^2) \tag{22}$$

Now the wave profile can be written as

$$\zeta = \zeta_1 + \zeta_2 \tag{23}$$

After calculating the fluid velocity $\nabla\Phi$ at the field points on the wetted surface, the pressure coefficient can be evaluated as

$$C_P = 1 - \left(\frac{\nabla\Phi}{U}\right)^2 \tag{24}$$

where

$$\nabla\Phi = \vec{U} + \nabla\phi,$$
$$where: \nabla\phi = \nabla\phi_1 + \nabla\phi_2 \tag{25}$$

Now, including the waterline integral, the lift and wave-making drag coefficients can be obtained as

$$C_W = -\frac{\sum_{i=1}^{N_B} C_P n_x \Delta S}{\sum_{i=1}^{N_B} \Delta S} = -\frac{\rho g \oint_{WL} \zeta^2 n_x dl}{\rho S U^2} \tag{26}$$

$$C_L = -\frac{\sum_{i=1}^{N_B} C_P n_y \Delta S}{\sum_{i=1}^{N_B} \Delta S} \tag{27}$$

where ΔS denotes the area of an element on the wetted surface.

4. NUMERICAL RESULTS

a) Various bodies

Many examples have been done by researchers during the past years. Here, we presented two types of lifting bodies and non-lifting bodies in this paper to show the capability of the method. The body is immersed like hydrofoil or surface piercing like strut and Wigley hull.

Hydrofoil and strut: We applied potential flow theory by the BEM technique with nonlinear free surface condition to the different bodies and present the free surface profile solutions. First, we applied the method for the hydrofoil with NACA4412 section. Mesh surface of the rectangular hydrofoil is shown in Fig. 2. The number of elements is selected 900 on the body and 3200 on the free surface. Our computational effort indicates these element numbers are enough for obtaining the numerical solutions. The potential and pressure distribution on the rectangular hydrofoil are shown in Figs. 3 and 4, respectively. The results are given at Froude number $Fn = 1.0$, depth ratio $H/C = 1.0$, aspect ratio $AR = 10$, and attack angle

$\alpha = 5[\text{deg.}]$. Froude number of the foil is defined as $Fn = U/\sqrt{gC}$, where C is chord length. Comparison of the pressure distribution shows good agreement between the present method and Yeung & Bouger data [21]. Hydrofoil lift and wave-making drag coefficients are determined by the present method and some results are compared with the other computational data.

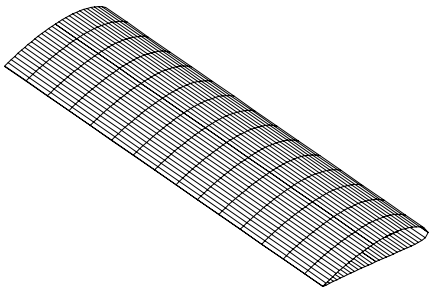

Fig. 2. Mesh surface of the rectangular hydrofoil (NACA4412, Number of elements = $N_{Tot} = 900$)

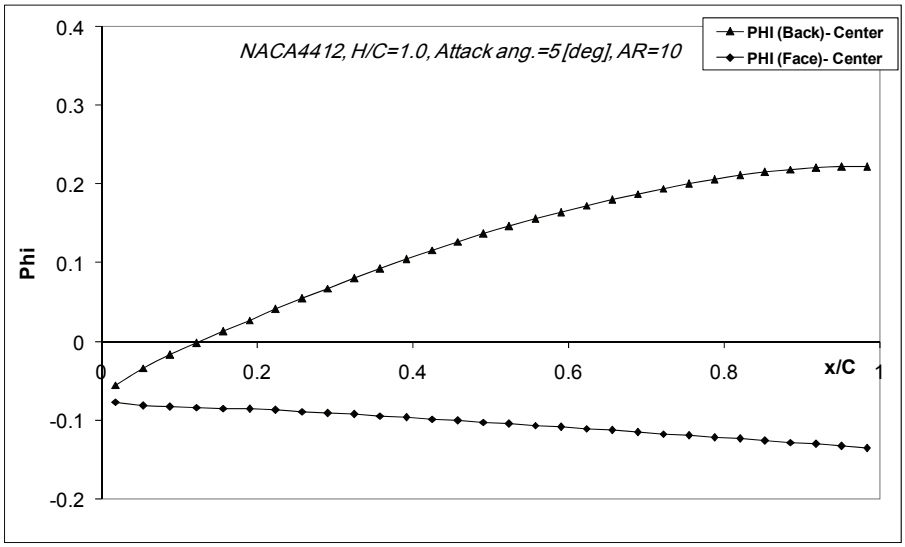

Fig. 3. Potential distribution on the rectangular hydrofoil,
$Fn = 1.0,\ H/C = 1.0,\ AR = 10,\ \alpha = 5(\text{deg.})$

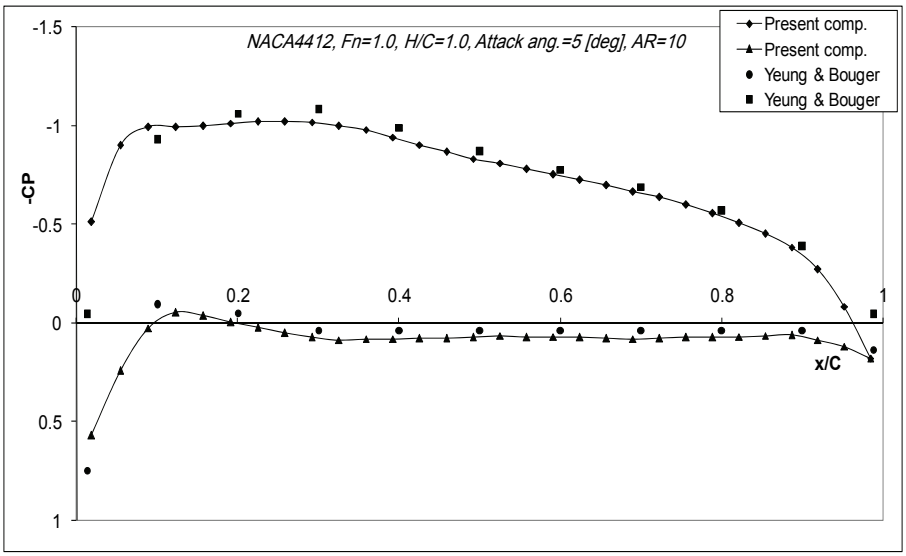

Fig. 4. Comparison of pressure distribution on the rectangular hydrofoil,
$Fn = 1.0,\ H/C = 1.0,\ AR = 10,\ \alpha = 5(\text{deg.})$

The wave-making resistance and lift are easily obtained by integrating hulls surface pressure. Variations in lift and wave drag coefficients with the Froude number for a NACA0012 profile for various positions below the free surface are compared in Figs. 5 and 6 with Uslu & Bal's numerical results [11]. The aspect ratio is 10, and is nearly defined 2-dimensional foil. Also, Figs. 7 and 8 show comparison of the lift and wave-making drag coefficients of the rectangular hydrofoil (NACA4412 profile) at H/C=1.0, $AR = 6$, $\alpha = 5(\text{deg.})$. The maximum value of the lift coefficient occurs at Froude number of about 0.5 and wave-making drag coefficient is observed at Froude number of about 0.8. Good correlations have been obtained between the present results and other numerical data.

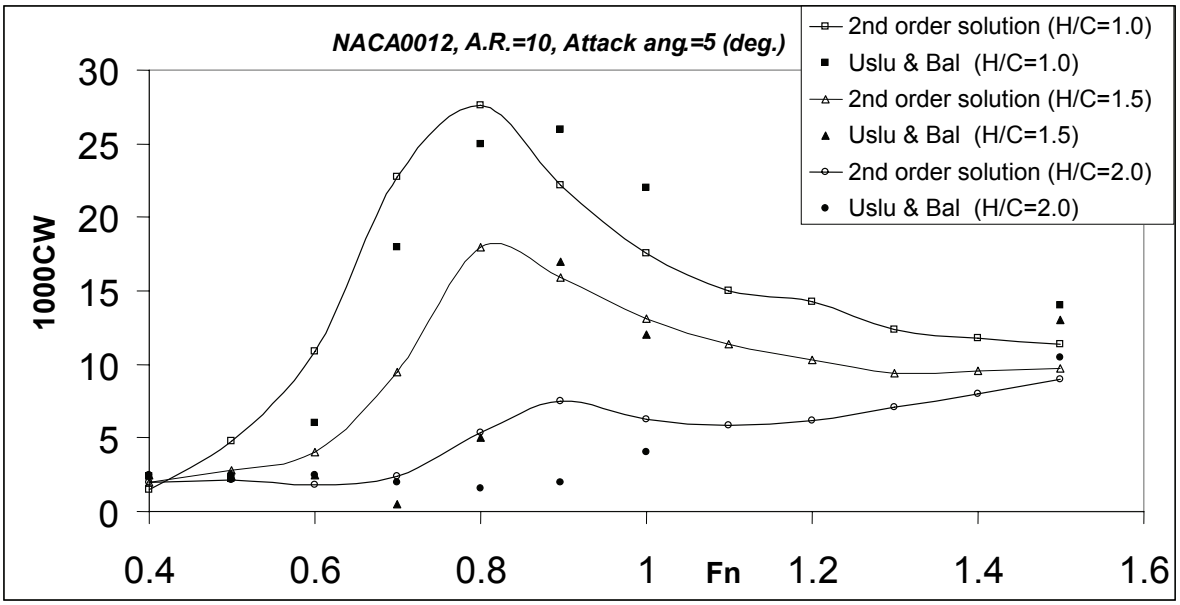

Fig. 5. Variations in wave-making drag coefficient with the Froude number for a NACA0012 profile for various positions below the free surface

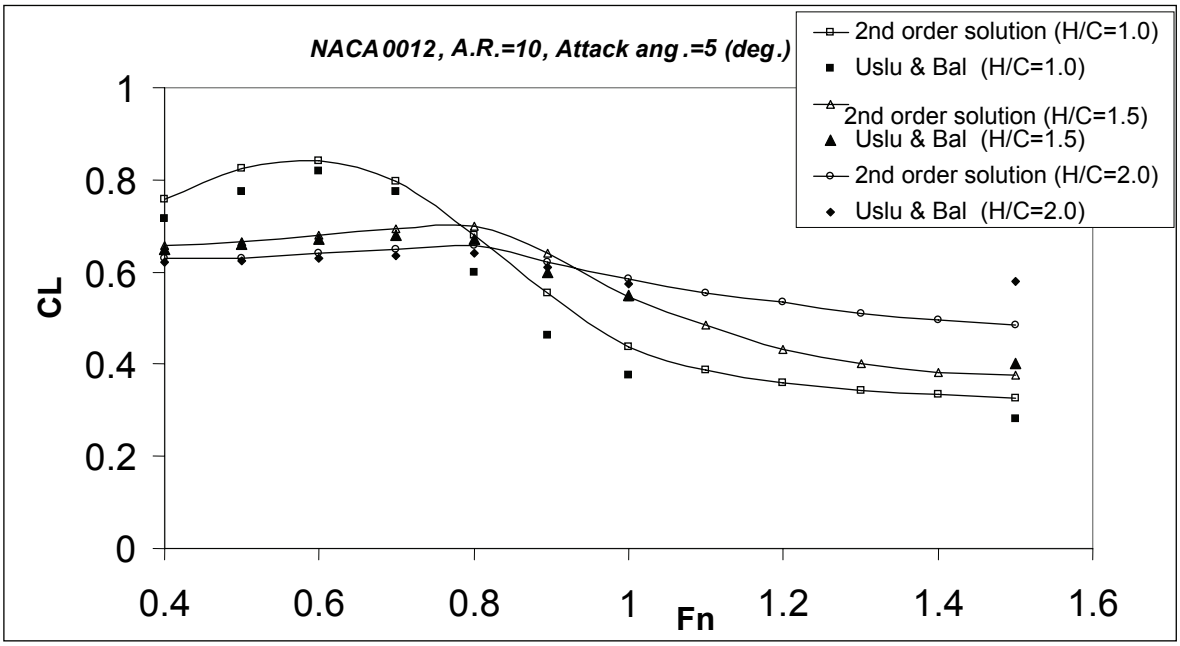

Fig. 6. Variations in lift coefficient with the Froude number for a NACA0012 profile for various positions below the free surface

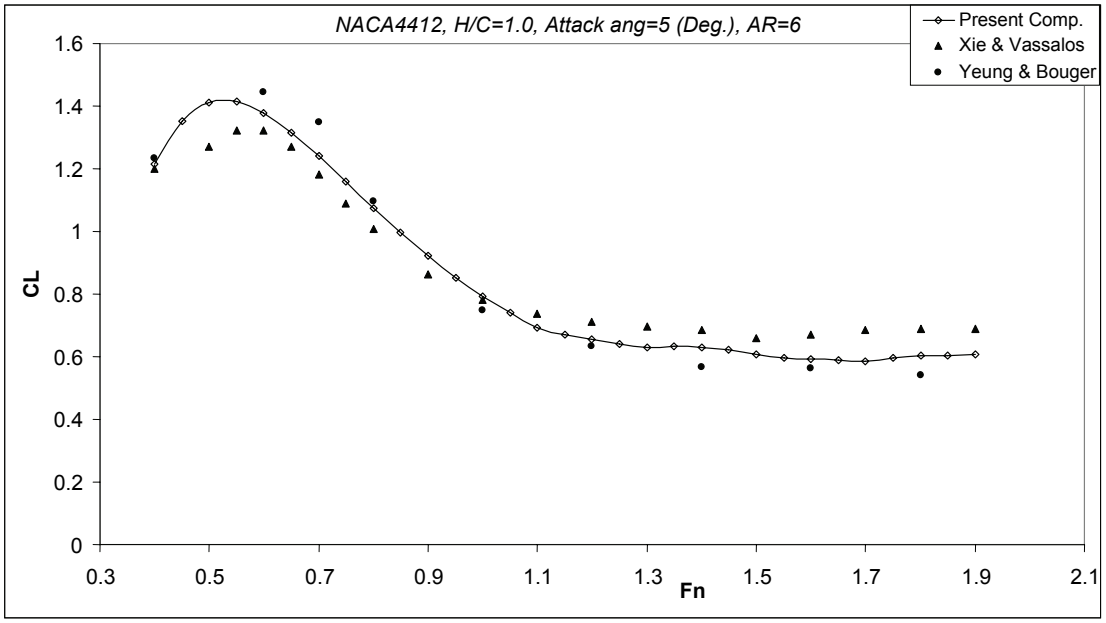

Fig. 7. Comparison of lift coefficient of the rectangular hydrofoil, $H/C=1.0,\ AR=6,\ \alpha=5(\text{deg.})$

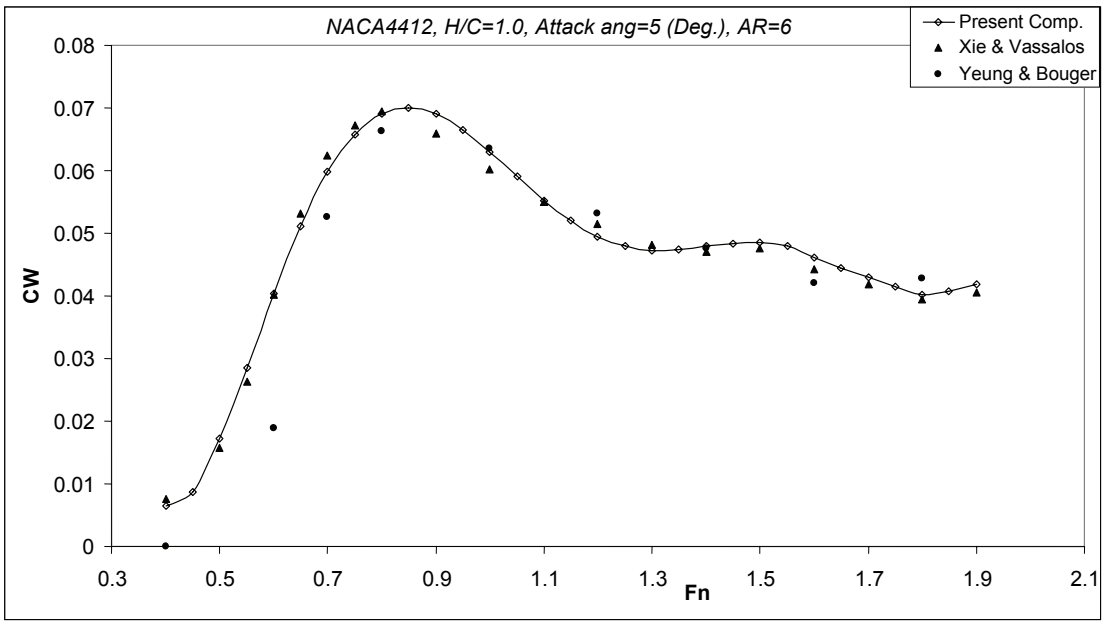

Fig. 8. Comparison of wave-making drag coefficient of the rectangular hydrofoil, $H/C=1.0,\ AR=6,\ \alpha=5(\text{deg.})$

The wave pattern on the hydrofoil with NACA4412 is shown in Figs. 9 and 10. In these figures, two different families of waves (transverse waves and short-length divergent waves) can be easily observed. We extended an example in Fig. 11 for special hydrofoil (like two moving parallel bodies or two parallel moving pressures) at *Fn=0.40*. The *V*-shape of the waves downstream becomes, in that case, a *W*-shape. This case can be viewed as the wave interactions between ships moving parallel in deep water.

Another example is presented for the strut or rudder. Figures 12 and 13 illustrate the free surface elevation on the strut with the *NACA0012* section at two Froude numbers, 0.3 and 0.4. When F_n increases,

the amplitude of the divergent waves becomes more important than that of the transverse waves. The wavelength of the transverse wave increases with the Froude number.

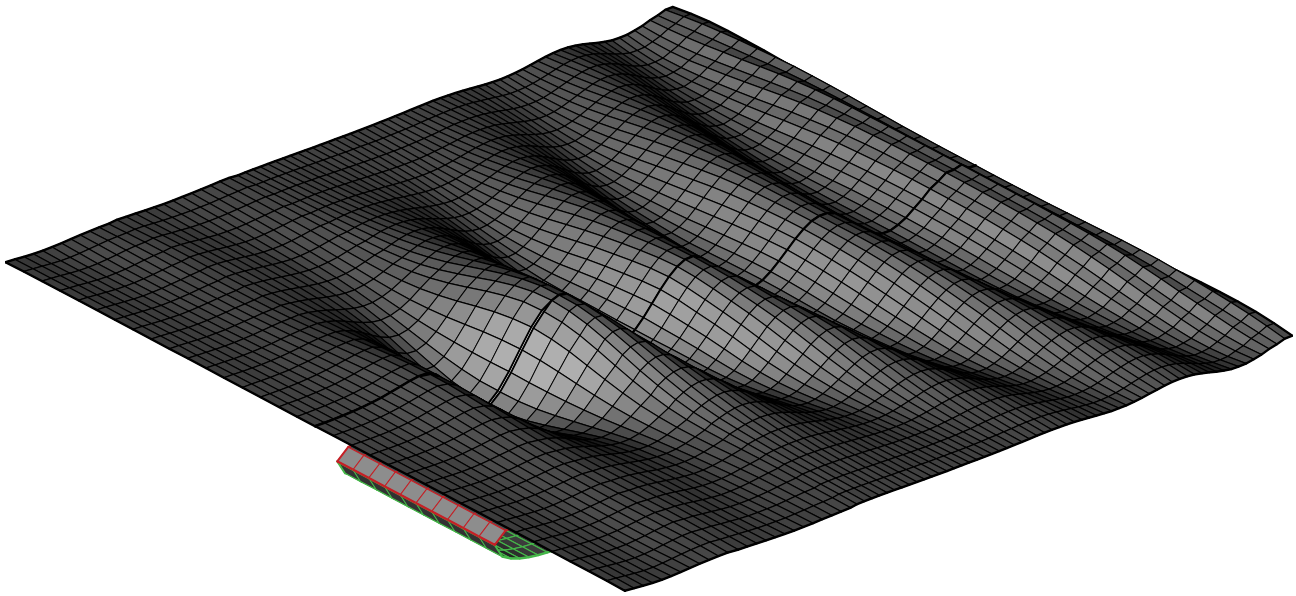

Fig. 9. Wave pattern on the hydrofoil with NACA4412
($Fn = 0.3,\ H/C = 0.3,\ AR = 1.0,\ \alpha = 5(\text{deg.})$)

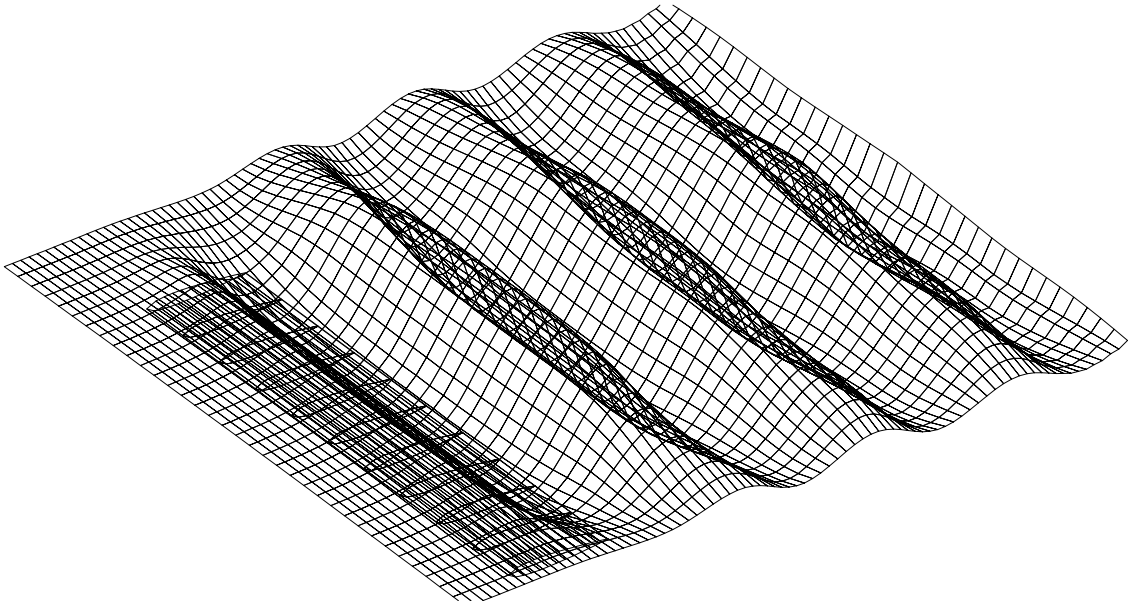

Fig. 10. Wave pattern on the rectangular NACA4412 profile hydrofoil
($Fn = 0.5,\ H/C = 0.3,\ AR = 4.0,\ \alpha = 5(\text{deg.})$)

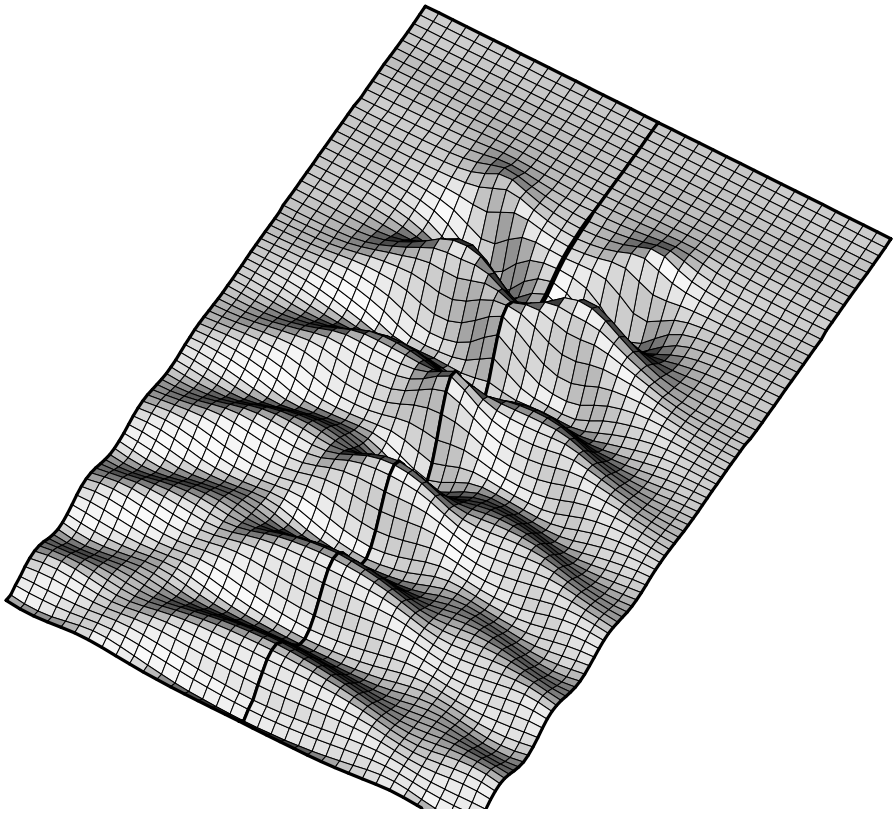

Fig. 11. Free surface pattern on the special hydrofoil (like two moving parallel bodies) (*Fn=0.40*)

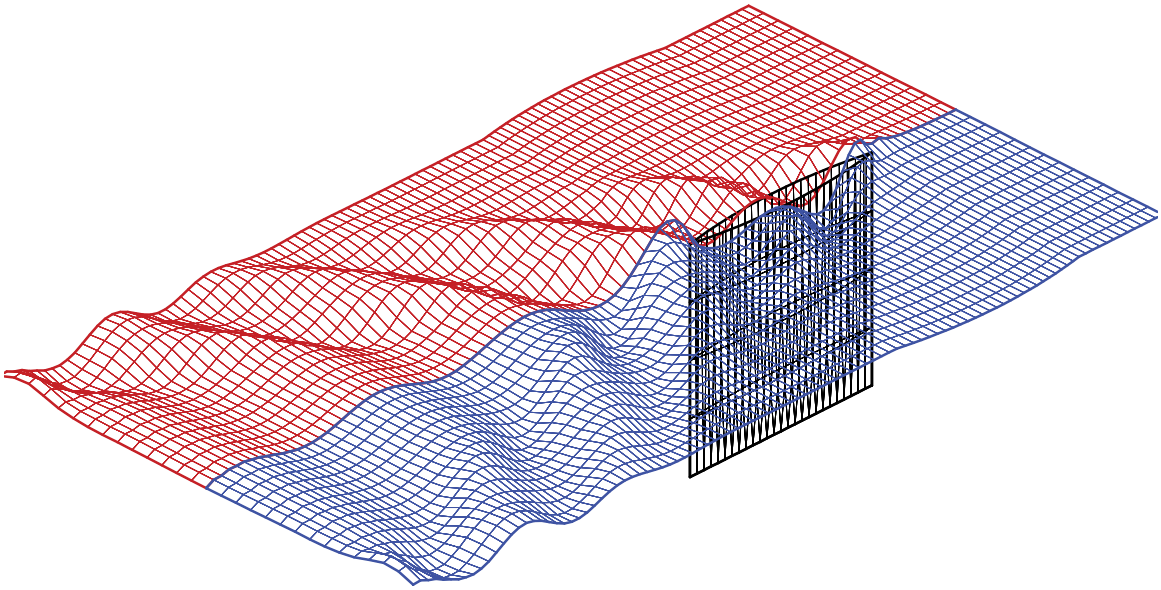

Fig. 12. Free surface elevation on the strut with NACA0012 section, (*Fn=0.3*)

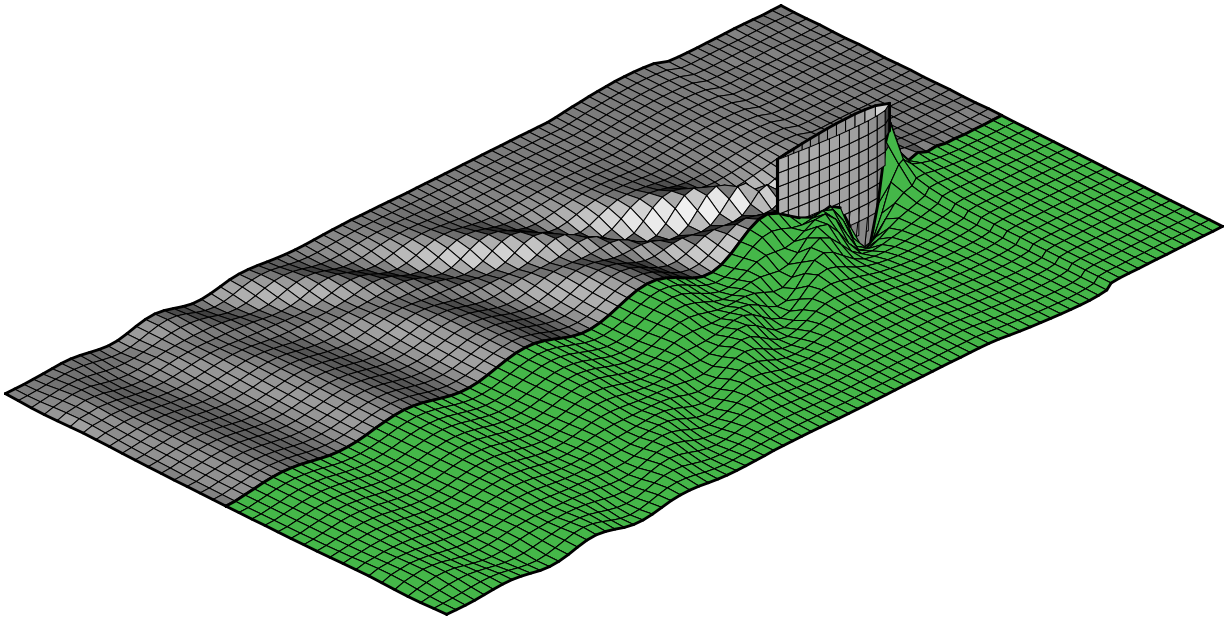

Fig. 13. Free surface elevation on the strut with NACA0012 section, (*Fn=0.4*)

Wigley hull: The method is extended to the standard Wigley hull. Its geometric surface is mathematically defined as

$$y = \pm\frac{B}{2}\left[1-\left(\frac{2x}{L}\right)^2\right]\left[1-\left(\frac{z}{T}\right)^2\right] \tag{28}$$

where L is the hull length, B the full hull beam and T the hull draft. For the standard Wigley hull used in this computation, the length-to-beam ratio L/B is 10 and the beam-to-draft ratio B/T is 1.6. The computed wave patterns for the standard Wigley hull at Froude number 0.26 and 0.3 are shown in Figs. 14 and 15. These are three dimensional views of the free surface. There are no wave reflections at the side- and downstream-boundaries since they are open boundaries for the computational domain. Figure 16 presents the comparisons of the wave elevations along the Wigley hull between the experimental measurements and the numerical results (1-st and 2-nd order) from the current solutions for Froude numbers 0.250, 0.267, 0.289 and 0.316, respectively. The nonlinear numerical values agree well with the experimental measurements [20] over the series of Froude numbers considered. The nonlinear calculations indicate significant approximation to the actual free surface elevations along the hull, and the wave profiles are quite smooth.

Figure 17 shows the comparison of the pressure coefficient along Wigley with the experimental data, the same Froude numbers with wave elevation. The numerical results for non-linear free surface also agree well with the experimental data of both free surface elevations and pressure distributions for the Wigley hull. In Fig. 18, the 1st and 2nd order present numerical result of wave-making resistance of the Wigley hull is compared with those of experiments given by Nakos and Sclavounos [9]. The wave resistance curve indicates a good match with respect to the Froude number and is reliable with the experimental measurements.

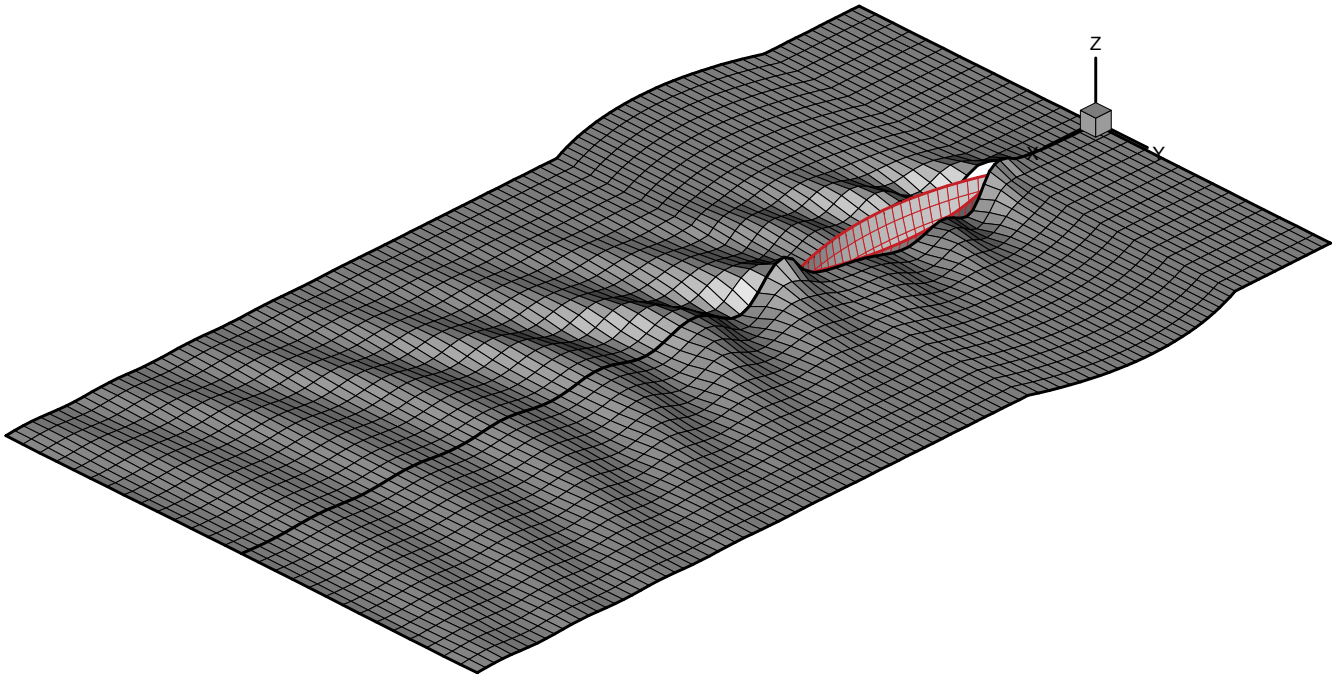

Fig. 14. Free surface elevation on the Wigley hull, (*Fn=0.26*)

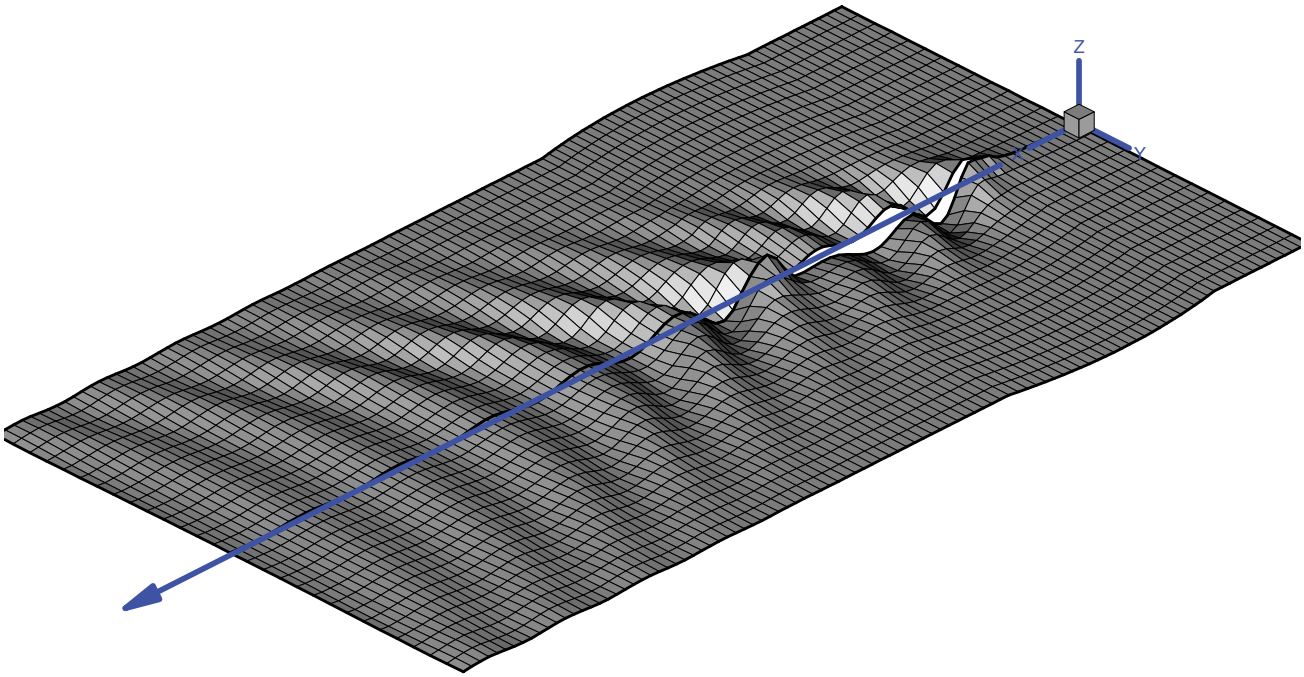

Fig. 15. Free surface elevation on the Wigley hull, (*Fn=0.30*)

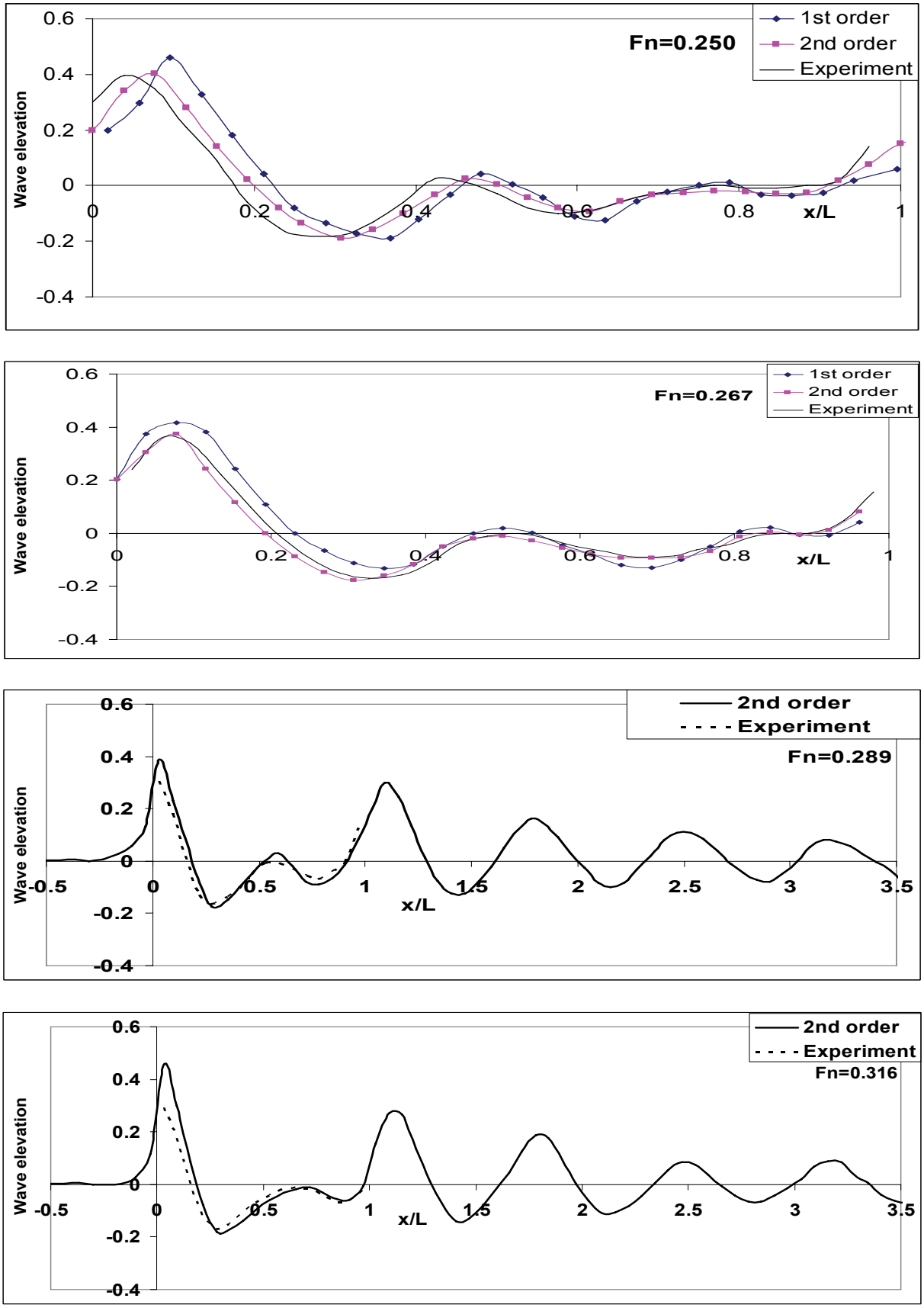

Fig. 16. Comparisons of wave elevation along Wigley hull at various Froude numbers (*Fn*)

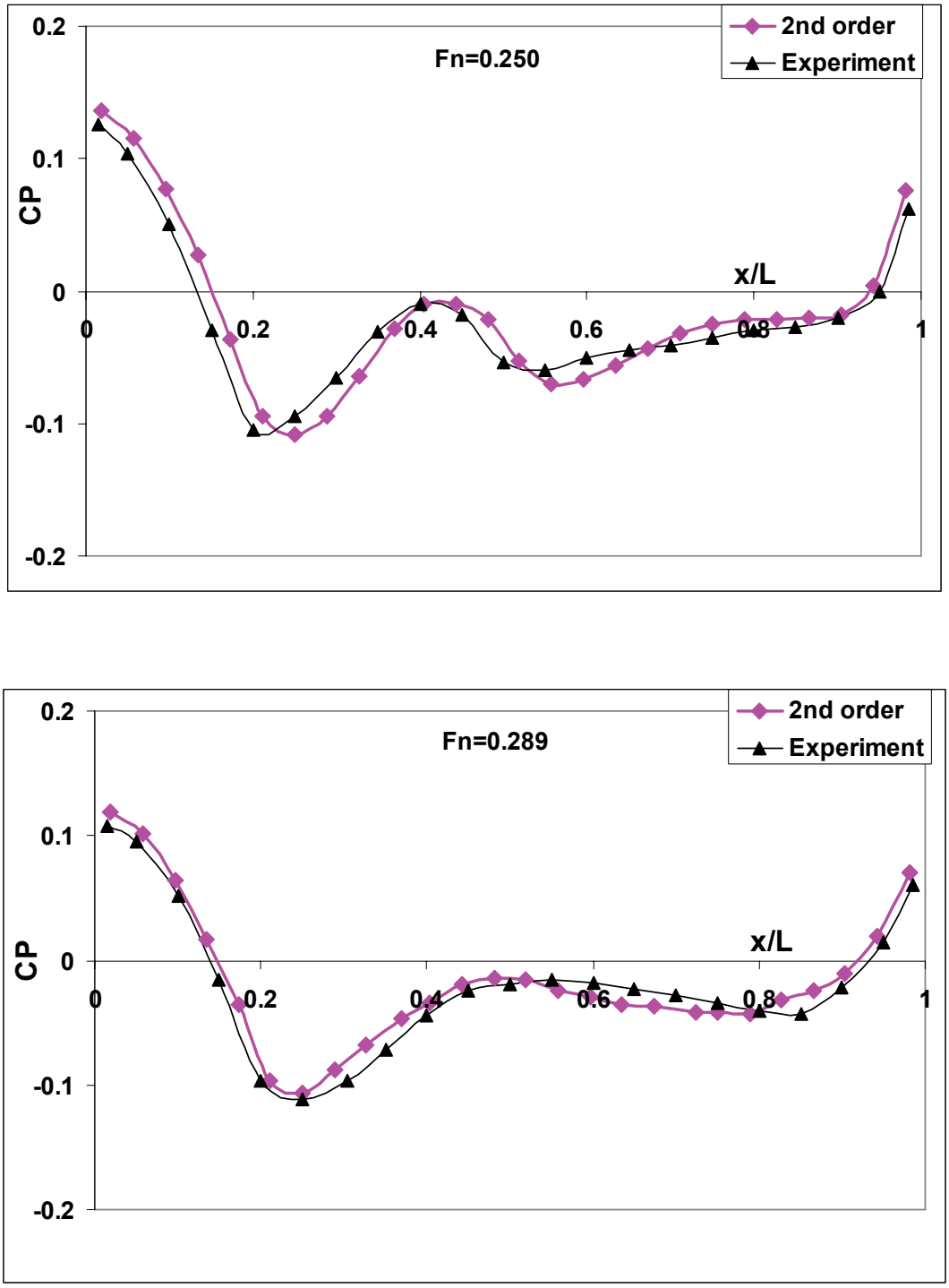

Fig. 17. Comparisons of pressure coefficient along Wigley at various Froude numbers (*Fn)*

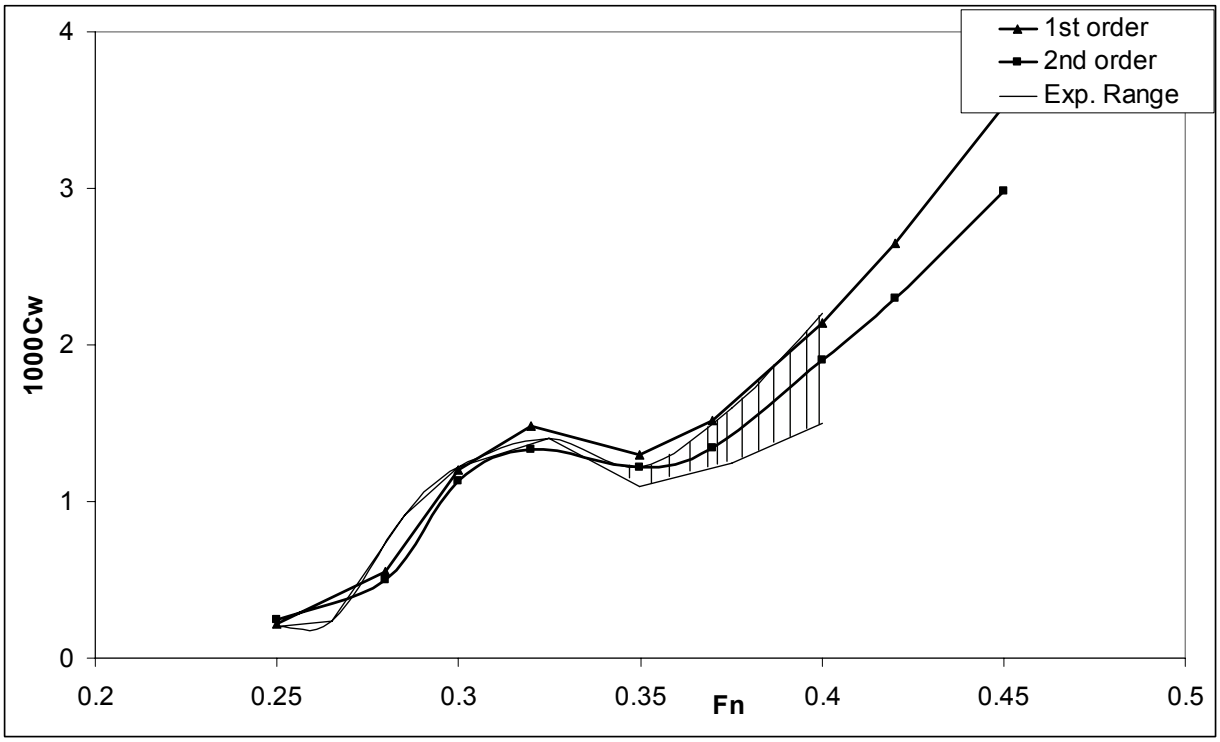

Fig. 18. Comparison of the wave-making resistance of the Wigley hull

5. CONCLUSION

We have calculated three dimensional wave pattern of the three dimensional various bodies which moves in the immersed or surface piercing conditions. The first and second order free-surface boundary conditions are employed. The method has been applied to a variety of computational cases and compared with experimental measurements and other numerical results for the pressure distribution, lift and wave-making drag. It is shown that satisfactory agreement and accuracy can be achieved by second order solutions. The three-dimensional wave patterns present a clear and apparent view of the characteristics of free surface wave.

Acknowledgments- The authors wish to thank all three reviewers for many comments and suggestions to update and modify the present paper.

NOMENCLATURE

AR	aspect ratio
B	breadth of the ship
C	chord length
C_P	pressure coefficient
C_W	wave-making drag
C_L	lift coefficient
F_n	Froude number
g	gravitational acceleration
G	Green's function
H	depth of the hydrofoil from free surface
H/C	pth-chord ratio

L	length of the ship
T	draft of the ship
N_B	number of elements on the body and
N_F	number of elements on the free surfaces
N_W	number of elements on the trailing vortex wake surface
M	number and spanwise of the hydrofoil
N_B	total number of elements on the body
N_F	total number of elements on the free surface
N_T	total number of elements
$\vec{r}$	distance between the singular point p to integration point q
$\vec{r}'$	distance between the singular point p to image integration point q′
$\vec{U}$	inflow velocity
$\vec{X}(p)$	position vector
K_0	wave number
$\vec{n} = (n_x, n_y, n_z)$	outward unit normal vector
P_{TE}^{BS}	pressure at back side of TE
P_{TE}^{FS}	pressure at face side of TE
S_B	surface of the body
S_F	surface of the free surface
S_W	surface of the TVW
DB_{ij}, SB_{ij}	influence coefficient of source, double on the body
DW_{ijl}, SF_{ij}	influence coefficient of double and source on the wake and free surface
$\partial\phi / \partial n$	normal derivative of the velocity potential
$\zeta(x, y)$	wave elevation
$\Phi(x, y, z)$	total velocity potential
(u, v, w)	local coordinate system
(x, y, z)	global coordinate system
Φ_x, Φ_y, Φ_z	derivative of velocity potential relative to x, y and z-directions
ϕ_{1z}	first order of the first derivative of the potential in z-direction
ϕ_{2z}	second order of the first derivative of the potential in z-direction
ϕ_{1xx}	first order of the second derivative of the potential in x-direction
ϕ_{2xx}	second order of the second derivative of the potential in x-direction
ζ_x, ζ_y	derivative of the wave elevation relative to x and y-directions
ϕ	perturbation potential
ϕ_{in}	free stream velocity potential
ΔS	area of an element
δ_{ij}	Kronecker delta function
σ	source strength on each free surface element
ρ	density of the water
α	attack angle
$\Delta\phi$	difference of the velocity potential at TE
$\nabla\phi_1$	differentiation of potential
TE	trailing edge
TVW	trailing vortex wake

REFERENCES

1. Wehausen, J. V. (1973). *The wave resistance of ships*. Advances in Applied Mechanics, Vol. 13, pp. 93–245.
2. Newman, J. N. (1977). *Marine hydrodynamics*. MIT Press: Cambridge, MA, U.S.A.
3. Scullen, D. C. & Tuck, E. O. (1996). Three-dimensional steady state nonlinear free-surface flow computation. *Gazette of the Australian Mathematical Society*, Vol. 23, pp. 80-84.
4. Tuck, E. O. & Scullen, D. C. (2002). A comparison of linear and nonlinear computations of waves made by slender submerged bodies. *Journal of Engineering Mathematics*, Vol. 42, pp. 252-264.
5. Cao, Y., Schultz, W. W. & Beck, R. F. (1991). Three dimensional desingularized boundary integral methods for potential problems. *Int. J. for Numer. Meth. Fluids*, Vol. 12, pp. 785-803.
6. Forbes, L. K. (1989). An algorithm for 3-dimensional free-surface problems in hydrodynamics. *Journal of Computational Physics*, Vol. 82, pp. 330-347.
7. Parau, E., Vanden-Broeck, J. M. (2002). Nonlinear 2D and 3D-dimensional free surface flows due to moving disturbances. *European Journal of Mechanics B/Fluids*, Vol. 21, pp. 643–656.
8. Grilli, S. T., Guyenne, P. & Dias, F. (2001). A fully nonlinear model for three-dimensional overturning waves over arbitrary bottom. *Int. J. for Numer. Meth. Fluids*, Vol. 35, pp. 829-867.
9. Nakos, D. & Sclavounos, P. (1991). Ship motions by a three-dimensional Rankine panel method. *Proc. 18th Symp. Naval Hydro., Ann Arbor, August 1990*, (National Academy Press, Washington D. C.), pp. 21-40.
10. Bal, S. (2008). Prediction of wave pattern and wave resistance of surface piercing bodies ay a boundary element method. *International Journal for Numerical Methods in Fluids*, Vol. 56, pp. 305-329.
11. Uslu, Y. & Bal, S. (2008). Numerical prediction of wave drag of 2-D and 3-D bodies under or on a free surface. *Turkish J. of Eng. and Environmental Science*, Vol. 32, pp.177-188.
12. Xie, N., Vassalos, D. (2007). Performance analysis of 3D hydrofoil under free surface. *Ocean Engineering*, Vol. 34, pp.1257–1264.
13. Kara, F., Tang, C. Q. & Vassalos, D. (2007). Time domain three-dimensional fully nonlinear computations of steady body–wave interaction problem. *Ocean Engineering*, Vol. 34, pp.776–789.
14. Ghassemi, H., Ghiasi, M. & Ghamari, I. (2008). Nonlinear generated wave pattern due to three dimensional moving bodies. *Proceeding of the 8th Int. Conf. of Hydrodynamics (ICHD2008)*, Nantes, France.
15. Ghassemi, H., Kohansal, A. R. & Ghamari, I. (2009). Nonlinear free surface flows due to the lifting and non-lifting moving bodies. *17th Annual (International) Conference on Mechanical Engineering- ISME2009*, Tehran, Iran.
16. Ghassemi, H., Kohansal, A. R. & Ardeshir, A. (2009). Higher order boundary element method applied to the hydrofoil beneath the free surface. *Proceedings of the 28th International Conference on Ocean, Offshore and Arctic Engineering (OMAE2009)*, Honolulu, Hawaii, USA.
17. Seif, M. S. & Amini, E. (2004). Performance comparison between planning monohull and catamaran at high froude numbers. *Iranian Journal of Science & Technology, Transaction B, Engineering*, Vol. 28, No. B4, 2004.
18. Tarafder, S. & Suzuki, K. (2007). Computation of wave- making resistance of a catamaran in deep water using a potential-based panel method. *Ocean Engineering*, Vol. 34, pp.1892–1900.
19. Ghassemi, H. & Kohansal, A. R. (2009). Numerical evaluation of various levels of singular integrals, arising in BEM and its application in hydrofoil analysis. *Applied Mathematics and Computation*, Vol. 213 pp.277–289.
20. Kajitani, H., Miyata, H., Ikehata, M., Tanaka, H. & Adachi, H. (1983). Summary of the cooperative experiment on Wigley parabolic model in Japan. *Proceedings of the Workshop on Ship Wave Resistance Computations*, pp. 5–35.
21. Yeung, R. W. & Bouger Y. C. (1979). A hybrid-integral equation method for steady two-dimensional ship waves. *Int. J. Num. Meth. Eng*., Vol. 14, pp. 317-336.